A Novel Highly Dynamic Torque Control Scheme for Electrically Excited Synchronous Machines

Leonard Geier
Elektrotechnisches Institut (ETI)
Karlsruhe Institute of Technology (KIT)
Karlsruhe, Germany
leonard.geier@kit.edu

Stephan Goehner
Elektrotechnisches Institut (ETI)
Karlsruhe Institute of Technology (KIT)
Karlsruhe, Germany
stephan.goehner@kit.edu

Johannes Stoss
Elektrotechnisches Institut (ETI)
Karlsruhe Institute of Technology (KIT)
Karlsruhe, Germany
johannes.stoss@kit.edu

Dr.-Ing. Andreas Liske
Elektrotechnisches Institut (ETI)
Karlsruhe Institute of Technology (KIT)
Karlsruhe, Germany
andreas.liske@kit.edu

Prof. Dr.-Ing. Marc Hiller
Elektrotechnisches Institut (ETI)
Karlsruhe Institute of Technology (KIT)
Karlsruhe, Germany
marc.hiller@kit.edu

***Abstract*—In this work a novel torque control method for electrically excited synchronous machines (EESM) is presented that enables an increase in dynamics. This is achieved by utilizing the magnetic coupling between the exciter and the stator winding. For this only a modified operating point controller (OPC) is needed that selects current set values in dependence of the current state and the set torque. The OPC is combined with an PI-current controller. The proposed method also handles highly utilized EESMs with nonlinear magnetics including (cross-) saturation in all components. The effectiveness of the controller is verified by testbench measurements.**

***Index Terms*—electrically excited synchronous machine, wound rotor synchronous machine, non-linear control, torque control**

I. Introduction

The electrically excited synchronous machine (EESM) combines high power density, high efficiency and a high degree of safety. Additionally, EESMs are rare earth free which mitigates supply chain risks. For these reasons the interest in EESMs and their control systems has increased recently especially in the automotive industry.

The EESM's rotor flux can be adjusted through the excitation current i_e. Compared to the permanent magnet synchronous machine (PMSM) this results in an additional degree of freedom. The PMSM is described with the state variables (i_d,i_q) in a two-dimensional state space. A given set torque is reached on operating points that form a curve in the two-dimensional state space. In contrast, the EESM is modeled with three state variables (i_d,i_q,i_e) in a three dimensional state space. Here a given set torque can be achieved at operating points forming a surface in the three-dimensional state space.

Most EESM torque control schemes consist of two parts [1]–[5]. The first part is an operating point controller (OPC) which converts a given set torque to current set values. The second part is an underlying closed loop current controller that tracks the three current components.

The OPC selects an operating point from the corresponding set torque surface. Strategies that optimize for steady state efficiency have been investigated [2], [4], [5]. In these methods the rotor current needs to be adjusted in dependence of set torque and machine speed.

Closed-loop current controllers for EESMs have also been investigated. For highly dynamic current control, the magnetic coupling between the d- and e-axis and the magnetic non-linearity of highly utilized machines poses a challenge. A model predictive approach has been proposed in [6] which employs a non-linear flux model in form of a flux map. In [7], a non-linear PI-controller is used with a decoupling network based on a magnetic equivalent circuit. Both methods allow fast and accurate tracking of all three current components but are fundamentally limited by the available voltage.

In published EESM designs for electric vehicles a large exciter inductance is used which is often magnitudes larger than the stator inductances [2], [4], [5], [8]. This causes the exciter dynamics to be much slower compered to the stator even when the controller is operating at the voltage limit. The combination of the efficiency optimized OPC that requires adjustments in the exciter current and the low exciter dynamics lead to reduced torque dynamics [4].

A theoretical analysis of this control problem has been carried out in [9] where a dynamic optimization problem has been solved to obtain a time optimal solution regarding torque and flux dynamics. The results show that compared to existing methods an increase in dynamic is possible by using the magnetic coupling between exciter and stator. In this work a real time capable implementation is proposed that uses the insights from the theoretical analysis. In the proposed scheme the improved dynamics are reached through a novel OPC. To track the currents an existing PI-controller is used [7].

This work starts with an introduction of the drive system

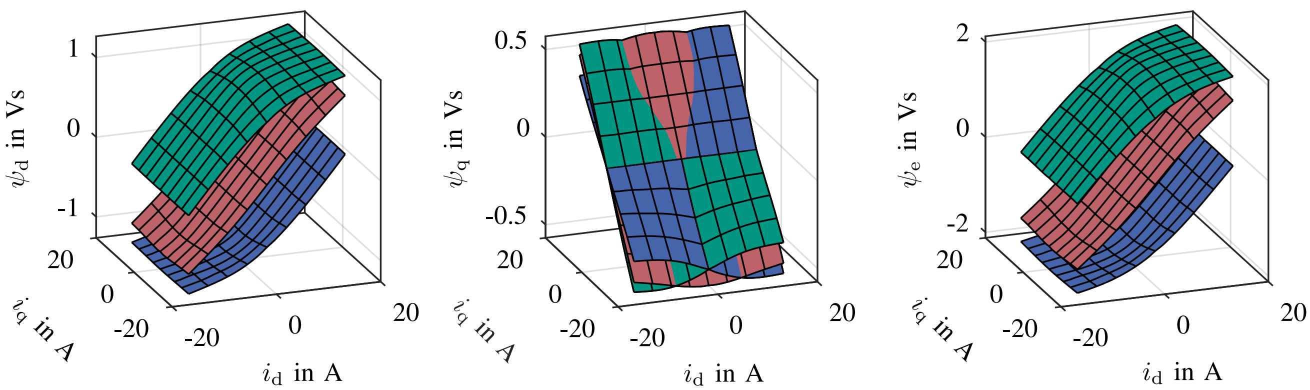

Fig. 1. Excerpt of an EESM flux map for $i_{\rm e} = -11$ A (blue), $i_{\rm e} = 0$ A (red) and $i_{\rm e} = 11$ A (green)

including the non-linear machine model in sec. II. Steady state operating points are calculated in sec. III before the proposed torque control scheme is described in sec. IV. Test bench measurement results are presented in sec. V.

II. Model of the EESM Drives System

The system under consideration consists of an EESM which is fed by voltage source inverters in stator and rotor. Slip rings are used to operate the rotor.

A. Non-Linear Machine Model in Rotor Orientation

By applying Clarke- and Park-transformation to the phase voltage equations, the stator dynamics of a three phase synchronous machine in rotor orientation are described with

$$v_{\rm d} = R_{\rm s} i_{\rm d} + \dot{\psi}_{\rm d} - \omega \psi_{\rm q} \tag{1}$$

$$v_{\rm q} = R_{\rm s} i_{\rm q} + \dot{\psi}_{\rm q} + \omega \psi_{\rm d} \tag{2}$$

The additional dynamics of the exciter are described by

$$v_{\rm e} = R_{\rm e} i_{\rm e} + \dot{\psi}_{\rm e} \tag{3}$$

In the above equations ψ_x are the flux, i_x the current and v_x the voltage components for stator d- and q-axis and exciter respectively. The resistance of stator and exciter are $R_{\rm s}$ and $R_{\rm e}$ and ω is the electrical frequency. In the following also the vector notation $\underline{i} = (i_{\rm d}, i_{\rm q}, i_{\rm e})$ and $\underline{\psi} = (\psi_{\rm d}, \psi_{\rm q}, \psi_{\rm e})$ is used.

The nonlinear magnetics including all couplings, saturation and cross-saturation are fully modeled using a three-dimensional flux map

$$f_{\psi} : \underline{i} \mapsto \underline{\psi} \tag{4}$$

which can be determined by finite element analysis or measurement [10]. An excerpt of the EESM flux map used in this work is shown in fig. 1.

With the number of pole pairs p the machine torque T is given by

$$T = \frac{3}{2} p (\psi_{\rm d} i_{\rm q} - \psi_{\rm q} i_{\rm d}) \tag{5}$$

Note that $\psi_{\rm d}$ predominantly depends on both the d- and e-current component due to magnetic coupling.

B. Inverter

The stator voltages are set by a two-level, three-phase inverter. To reduce complexity the stator voltage limit is set to

$$||(v_{\rm d}, v_{\rm q})|| \leq \frac{v_{\rm DC}}{\sqrt{3}} = v_{\rm s,max} \tag{6}$$

Dynamic overmodulation can be included in the following methods by modifying the voltage limit but will lead to results that depend on the rotor angle position as shown in [11] for a PMSM. As the dynamics are mostly limited by the exciter this simplification only has minor effects on the overall result.

The exciter is operated by a single-phase, full-bridge inverter via slip rings which results in a voltage limit of

$$|v_{\rm e}| \leq v_{\rm DC} = v_{\rm e,max} \tag{7}$$

III. Steady State Operating Points

For steady state operation the operating points with minimal ohmic losses are selected as proposed in [2]. For this the nonlinear optimization problem

$$\underline{i}_{\rm stat} = \underset{\underline{i}}{\rm argmin} \frac{3}{2} R_{\rm s} (i_{\rm d}^2 + i_{\rm q}^2) + R_{\rm e} i_{\rm e}^2 \tag{8}$$

$$s.t. \quad T(\underline{i}) = T^* \tag{9}$$

$$i_{\rm d}^2 + i_{\rm q}^2 \leq i_{\rm s,max}^2 \tag{10}$$

$$i_{\rm e} \leq i_{\rm e,max} \tag{11}$$

$$0 \leq i_{\rm e} \tag{12}$$

$$v_{\rm d}(\underline{i}, \omega)^2 + v_{\rm q}(\underline{i}, \omega)^2 \leq v_{\rm s,max}^2 \tag{13}$$

is solved numerically to obtain the current set values $\underline{i}_{\rm stat}$ for set torque T^* at speed ω. Due to symmetry in the flux map every torque value can be reached with a positive or a negative exciter current. To get a unique solution only positive exciter currents are allowed. The stator voltages are calculated using (1) and (2) for steady state operation and the torque is calculated by (5). Note that both calculations require the use of the flux map. A constraint that enforces the exciter voltage limit is not needed in steady state operation if $R_{\rm e} i_{\rm e,max} \leq v_{\rm e,max}$ is satisfied. The optimization is solved

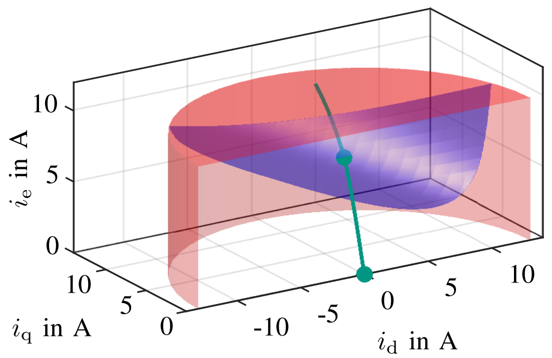

Fig. 2. In current space: steady state operating points (green), current limit (red), 10 Nm surface (blue)

for a grid of torque and speed values in the whole operating range. For use in a controller the results are stored in a lookup table (LUT)

$$\mathrm{LUT}_{\mathrm{stat,i}} : (T^*, \omega) \mapsto \underline{i}_{\mathrm{stat}} \tag{14}$$

The calculated steady state operating points in base speed operation form a line which is shown in current state space in fig. 2 and in flux state space in fig. 3 in green. For simplicity only positive set torque values are shown. Additionally, the current limit is shown in red and the surface with $T = 10$ Nm in blue. The steady state operating points for 0 Nm and 10 Nm are marked with green dots. The corresponding EESM was designed in [12], its flux map is shown in fig. 1 and the operating limits used are given in tab. II.

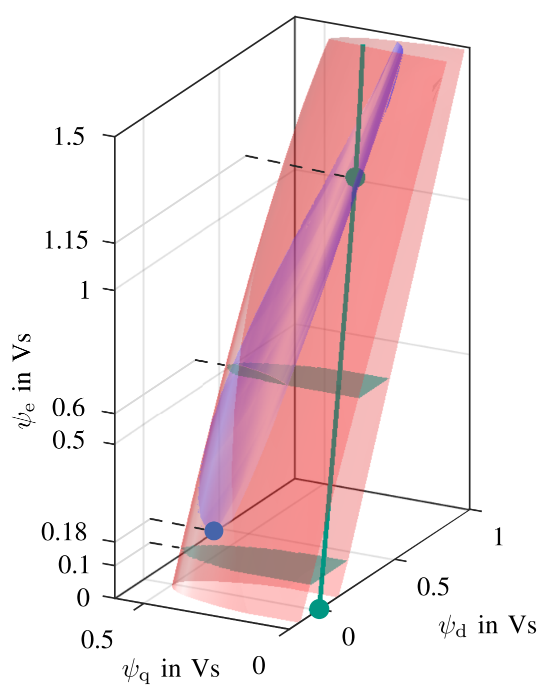

Fig. 3. In flux space: steady state operating points (green line), current limit (red), 10 Nm surface (blue), surfaces with $\psi_e = $ const. (green)

IV. Proposed Torque Control Scheme

In sec. IV-A the operating principle of the OPC in the proposed control system is motivated before the implementation is discussed in IV-B. For illustration the example of a torque step from 0 to 10 Nm is used.

A. Operating Principle

For a torque step all three current and flux components need to be changed as can be seen in fig. 2 and fig. 3. The operating points of the example are marked with green dots.

The response to a torque step is limited by the exciter dynamics which are much lower than the one of the stator. Limiting factor for the exciter current controller is the available voltage $v_{\mathrm{e,max}}$ which only allows a certain change in exciter flux $\Delta\psi_{\mathrm{e,max}} = \int_0^{\Delta t} v_{\mathrm{e,max}} - R_\mathrm{e} i_\mathrm{e} \mathrm{d}\tau$ per control period. Note that by this the exciter flux dynamics are limited – not the exciter current dynamics. Through the magnetic coupling the currents can be changed highly dynamic. This can be explained with the simplified linear flux relation $\psi_\mathrm{e} \approx L_\mathrm{e} i_\mathrm{e} + M i_\mathrm{d}$ with self and mutual inductance L_e and M. Both currents i_e and i_d can be changed highly dynamic under the condition that they are changed in opposite directions to keep the rate of flux change within the voltage limit. Thus the following description focuses on the flux components where the rate of exciter flux change is limited. With the much higher stator dynamics operating points where only the stator flux components ψ_d and ψ_q need to be adjusted can be reached quickly.

A geometrical visualization is given in fig. 3. Assuming the exciter flux is at $\psi_\mathrm{e} = 0.1$ Vs the corresponding plane with $\psi_\mathrm{e} = $ const. is shown in green. The operating points in the plane can be reached quickly while the plane itself can be moved up and down only slowly.

With the limited exciter dynamics the highest priority is to bring ψ_e to its value for steady state operation. For this the exciter voltage is saturated. In the example the plane of quickly reachable points therefore moves upwards from the start to the end point. During the transition favorable operating points in

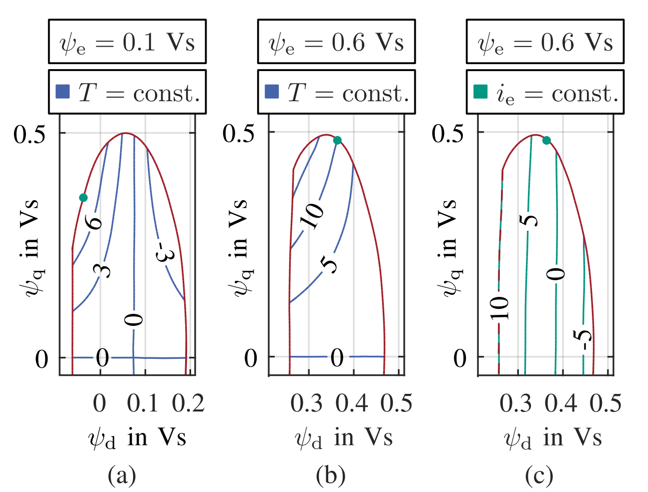

Fig. 4. $\psi_\mathrm{e} = $ const.-planes with: current limit (red) and lines of constant torque in Nm and exciter current in A

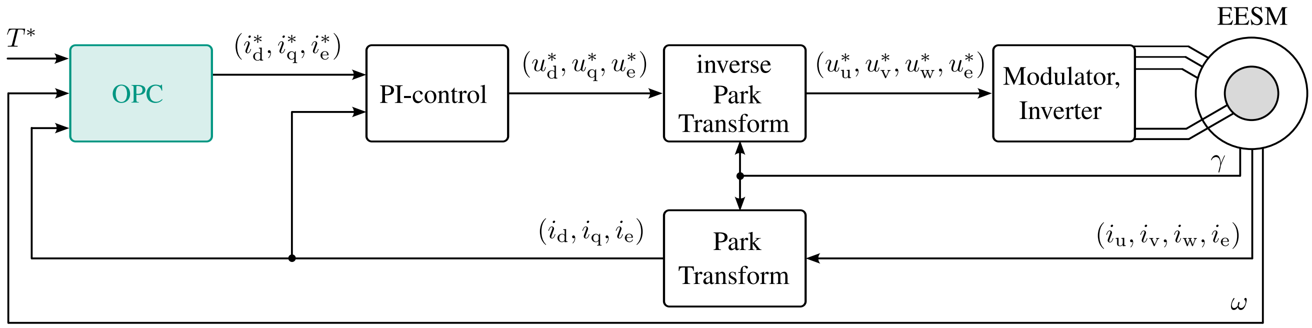

Fig. 5. Signal flow chart of torque control scheme composed of OPC and FOC current controller

the plane can be chosen. This degree of freedom can be used to increase the torque dynamics by selecting the operating point that minimizes the deviation from the set torque. Torques that can be reached at $\psi_{\mathrm{e}} = 0.1$ Vs are shown in fig. 4(a). The set torque of 10 Nm cannot be reached. Thus the operating point with maximum torque is selected which is marked in green.

When the exciter flux is increased to 0.18 Vs, T^* can be reached for the first time. This can be seen in fig. 3 where the corresponding operating point at the lower end of the T^*-surface is marked in blue.

During the following part of the transition form $\psi_{\mathrm{e}} = 0.18$ Vs to 1.15 Vs, T^* can be reached on a curve in the $\psi_{\mathrm{e}} = \mathrm{const.}$ plane. For $\psi_{\mathrm{e}} = 0.6$ Vs this is shown in fig. 4(b). By selecting a point from the curve, there is a degree of freedom for optimization. The points on the curve differ in the exciter current as can be seen in fig. 4(c) where lines of constant exciter current are shown. Consequently also the ohmic voltage drop $v_{\mathrm{e,R}} = R_{\mathrm{e}} i_{\mathrm{e}}$ varies and a favorable value can be chosen. For exciter flux build up the point with the lowest i_{e} and $v_{\mathrm{e,R}}$ is chosen which leaves a larger portion of the applied voltage for flux change. For flux decrease the point with highest i_{e} and $v_{\mathrm{e,R}}$ is selected to minimize $\dot{\psi}_{\mathrm{e}} = -v_{\mathrm{e,max}} - v_{\mathrm{e,R}}$. In the EESM designs [2], [4] $v_{\mathrm{e,R}}$ is in the range of 25-70% of $v_{\mathrm{e,max}}$ and thus has a significant impact on the flux dynamics.

B. Implementation of the Control Scheme

The proposed torque control is based on a field-oriented control (FOC) for the currents as depicted in fig. 5. A PI-controller with parameterization and decoupling as desribed in [7] is used. The control principle explained in sec. IV-A is implemented in the OPC. For this five LUTs are needed that are shown in tab. I.

$\mathrm{LUT}_{\mathrm{stat},\psi_{\mathrm{e}}}$ is defined by composition of $\mathrm{LUT}_{\psi_{\mathrm{e}}}$ and $\mathrm{LUT}_{\mathrm{stat,i}}$

$$\mathrm{LUT}_{\mathrm{stat},\psi_{\mathrm{e}}}(T^*, \omega) = \mathrm{LUT}_{\psi_{\mathrm{e}}}(\,\mathrm{LUT}_{\mathrm{stat,i}}(T^*, \omega)\,) \tag{15}$$

The operating point that are selected during transients are obtained from solving optimization problems numerically. The operating points with maximum torque from a plane with given exciter flux $\hat{\psi}_{\mathrm{e}}$ at a given speed ω are calculated by

$$\underline{i}_{\mathrm{T,max}} = \underset{\underline{i}}{\mathrm{argmax}}\; T(\underline{i}) \tag{16}$$

$$s.t. \qquad \psi_{\mathrm{e}}(\underline{i}) = \hat{\psi}_{\mathrm{e}} \tag{17}$$

$$i_{\mathrm{d}}^2 + i_{\mathrm{q}}^2 \leq i_{\mathrm{s,max}}^2 \tag{18}$$

$$|i_{\mathrm{e}}| \leq i_{\mathrm{e,max}} \tag{19}$$

$$v_{\mathrm{d}}(\underline{i}, \omega)^2 + v_{\mathrm{q}}(\underline{i}, \omega)^2 \leq v_{\mathrm{s,max}}^2 \tag{20}$$

where the constraints (18)-(20) ensure that current and voltage limits are respected. Analogously the points with the most negative torque are calculated by

$$\underline{i}_{\mathrm{T,min}} = \underset{\underline{i}}{\mathrm{argmin}}\; T(\underline{i}) \tag{21}$$

subject to the same constraints. Further, operating points with maximum i_{e} in a given exciter flux plane $\hat{\psi}_{\mathrm{e}}$ for set torque T^* and speed ω are calculated by

$$\underline{i}_{i_{\mathrm{e}},\mathrm{max}} = \underset{\underline{i}}{\mathrm{argmax}}\; i_{\mathrm{e}} \tag{22}$$

$$s.t. \qquad \psi_{\mathrm{e}}(\underline{i}) = \hat{\psi}_{\mathrm{e}} \tag{23}$$

$$T(\underline{i}) = T^* \tag{24}$$

$$i_{\mathrm{d}}^2 + i_{\mathrm{q}}^2 \leq i_{\mathrm{s,max}}^2 \tag{25}$$

$$|i_{\mathrm{e}}| \leq i_{\mathrm{e,max}} \tag{26}$$

$$v_{\mathrm{d}}(\underline{i}, \omega)^2 + v_{\mathrm{q}}(\underline{i}, \omega)^2 \leq v_{\mathrm{s,max}}^2 \tag{27}$$

LUT Name	**Mapping**	**Description**	**Source**
$\mathrm{LUT}_{\psi_{\mathrm{e}}}$	$\underline{i} \mapsto \psi_{\mathrm{e}}$	to get the exciter flux for measured currents	ψ_{e}-component of flux map in eq. (4)
$\mathrm{LUT}_{\mathrm{stat,i}}$	$(T^*, \omega) \mapsto \underline{i}_{\mathrm{stat}}$	to get the current set values for steady state operation	explained in sec. III, eq. (14)
$\mathrm{LUT}_{\mathrm{stat},\psi_{\mathrm{e}}}$	$(T^*, \omega) \mapsto \psi_{\mathrm{e}}$	to get the exciter flux for steady state operation	explained in sec. IV-B
$\mathrm{LUT}_{\mathrm{inc}}$	$(T^*, \omega, \psi_{\mathrm{e}}) \mapsto \underline{i}^*$	to get current set values during transient for increasing exciter flux	
$\mathrm{LUT}_{\mathrm{dec}}$	$(T^*, \omega, \psi_{\mathrm{e}}) \mapsto \underline{i}^*$	to get current set values during transient for decreasing exciter flux	

TABLE I
LUTS USED IN THE PROPOSED OPC

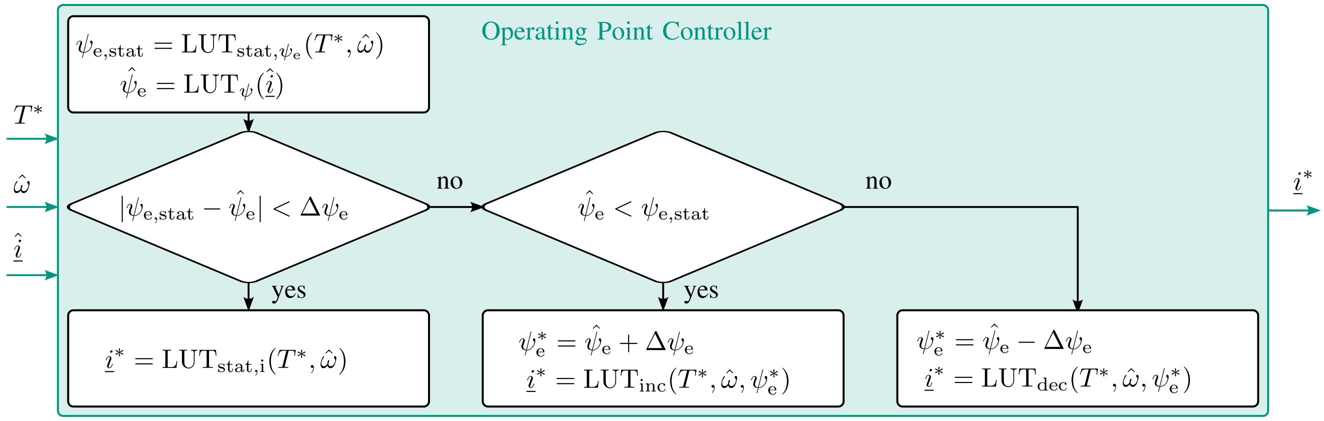

Fig. 6. Flow chart of the proposed OPC

Analogously points with minimum exciter current are calculated by

$$\underline{i}_{\mathrm{ie,min}} = \underset{\underline{i}}{\operatorname{argmin}}\, i_\mathrm{e} \tag{28}$$

subject to the same constraints.

$\mathrm{LUT}_{\mathrm{inc}}$ is constructed from the results of these optimizations problems. Therefore a grid for the variables T^*, ω and ψ_e is defined. For all combinations the solution to (28) is calculated and stored in the LUT. At the lower ψ_e-values the optimization does not have a solution for large $|T^*|$ values. For these instances the current vector with maximum torque from solving (16) is put in the LUT instead for $T^* > 0$ and the one with the most negative torque from (21) for $T^* < 0$. This way a case decision is implicitly contained in the LUT. If the flux is to be increased and a torque T^* is commanded the operating point with T^* and the lowest exciter current is output. If T^* cannot be reached at the current exciter flux, the operating point with maximum torque is output instead. Analogously $\mathrm{LUT}_{\mathrm{dec}}$ is calculated based on (22).

The structure of the OPC is shown as a flow chart in fig. 6. First the currently present value of exciter flux is calculated from the measured currents as well as the needed exciter flux for steady state operation with set torque and measured speed. To decide whether steady state or transient operation is present the difference between the two flux values is compared against a threshold value $\Delta\psi_\mathrm{e}$. The threshold is set to $\Delta\psi_\mathrm{e} = v_{\mathrm{e,max}}\Delta t$ where Δt is the sum of all delays in the underlying control loop. For stationary operation the corresponding set currents are output. For the transient case current set values are read form the respective LUT depending on whether the flux has to be increased or decreased. To ensure an increase or decrease of ψ_e with saturated exciter voltage, the exciter flux is adjusted by $\Delta\psi_\mathrm{e}$ before the LUT evaluation.

TABLE II
CHARACTERISTIC DATA OF THE EESM

Symbol	Meaning	Value
P_{max}	max. Power	5.9 kW
$i_{\mathrm{s,max}}$	max. stator current	13 A
$i_{\mathrm{e,max}}$	max. excitation current	10 A
$v_{\mathrm{s,DC}}$	stator DC link voltage	170 V
$v_{\mathrm{e,DC}}$	exciter DC link voltage	20 V

V. Measurement Results

The signal processing system used is based on a *Xilinx Zynq 7030* System-on-Chip and described in detail in [13]. The implementation is done by *MATLAB/Simulink* code generation. The controller runs at a frequency of 10 kHz. The measurements are carried out at constant speed which is ensured by a speed controlled PMSM. A picture of the test bench is shown in fig. 7. Torque is measured with a torque sensor *DRFL-III-150* from *ETH Messtechnik GmbH*. Characteristic data of the EESM is given in tab. II.

In fig. 8 - 11 the results of a step response from 0 Nm to 10 Nm at 200 rpm are shown. A comparison is given between the proposed OPC (black) and a state of the art OPC (green) that directly outputs the stationary operating point currents. Both methods use the same PI-current controller and the same operating limits. The flux curves have been calculated from the currents using the flux maps of fig. 1.

In the torque response it is clearly visible that the proposed method outperforms the reference controller. The oscillation in the torque signal can be explained by torque ripple of the motor and is not present in the currents. The trajectory of the proposed OPC in flux state space in fig. 8 shows the expected course. The exciter flux is continuously increased. For low ψ_e

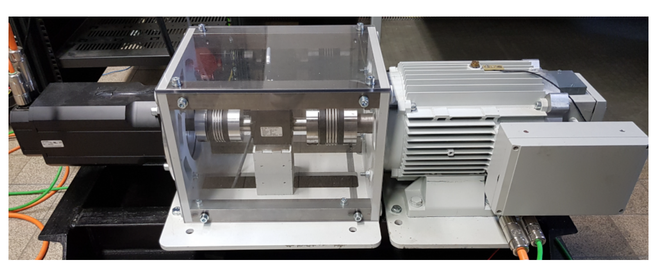

Fig. 7. Testbench - Dyno (left), EESM (right)

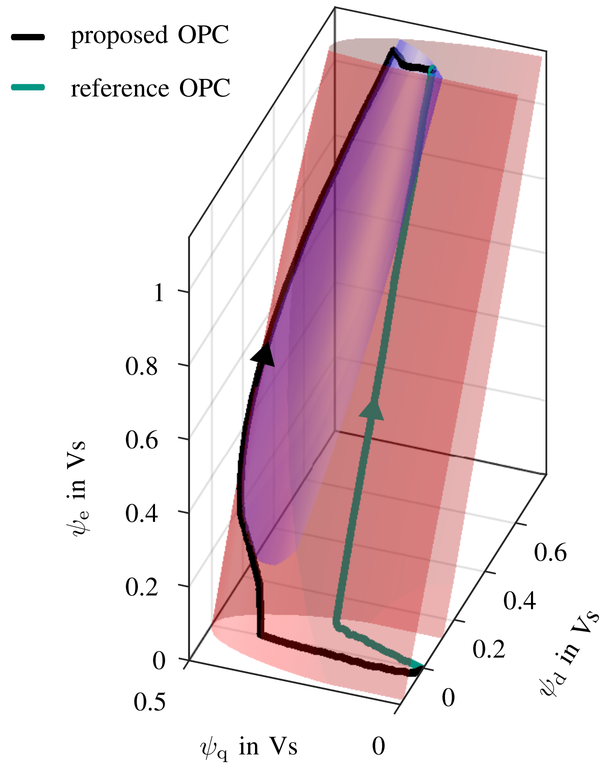

Fig. 8. T^*-surface (blue), current limit (red) and trajectory in flux space

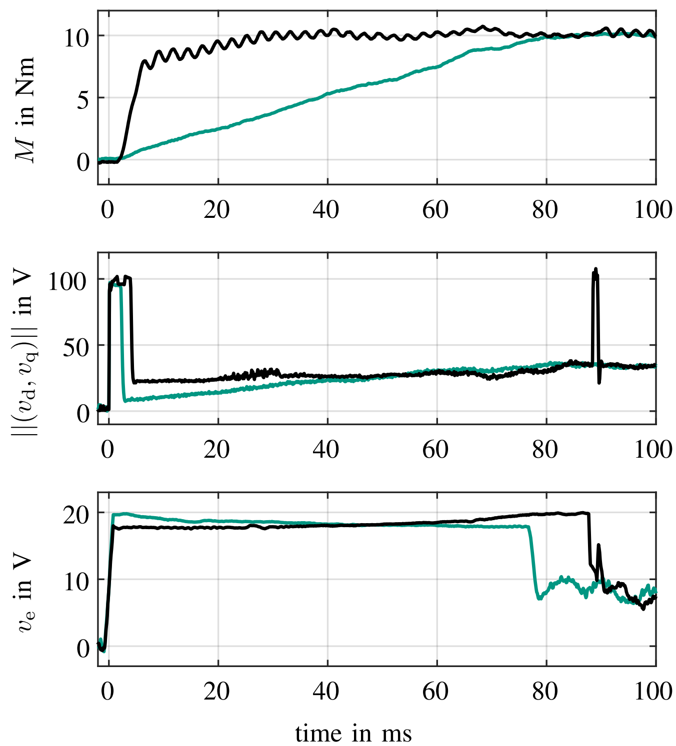

Fig. 10. Torque and voltage - optimization(black), reference controller (green)

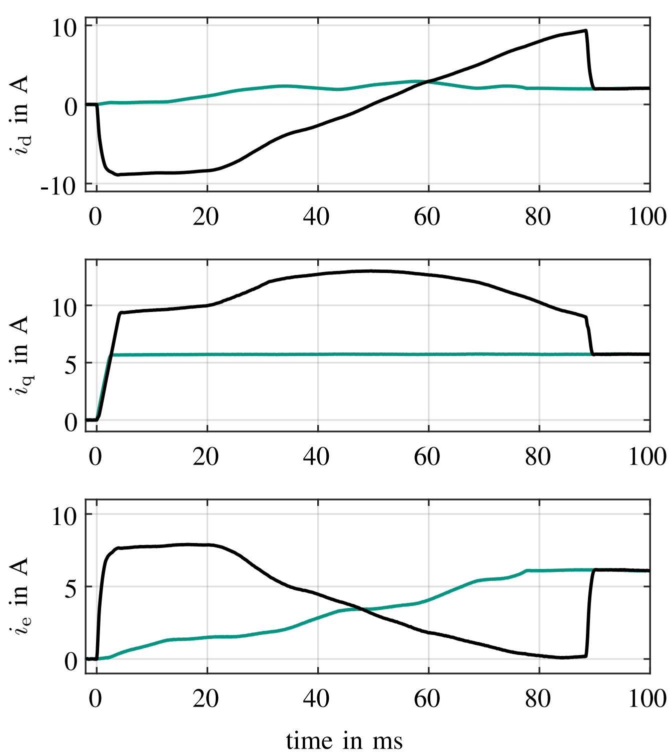

Fig. 9. Current - optimization (black), reference controller (green)

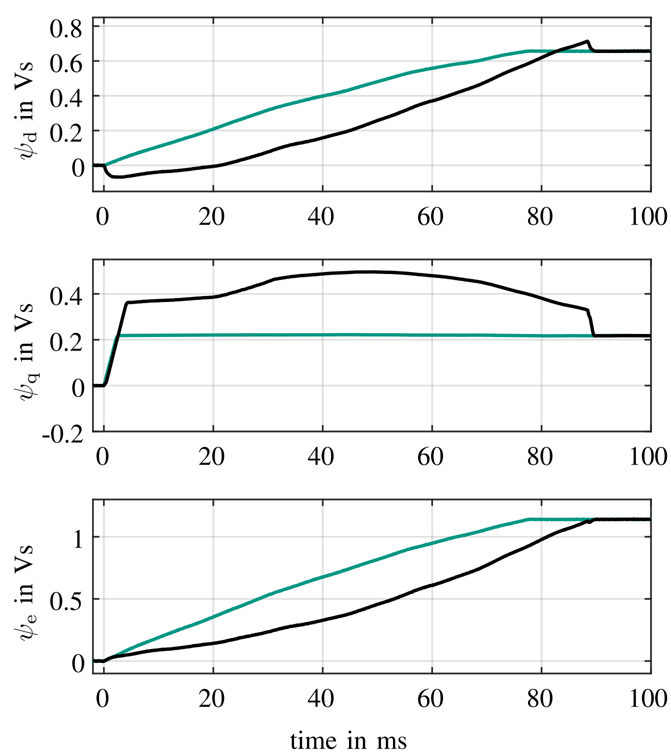

Fig. 11. Flux - optimization (black), reference controller (green)

it leads to the point with maximum possible torque at the current limit. After the T^*-surface is met at the lower end the trajectory follows the intersection of current limit and T^*-surface as the points with lowest i_e are chosen. The trajectory ends in the steady state operating point.

The measured curves show that the magnetic coupling is used to increase the exciter current quickly by decreasing the d-current which enables the fast torque response. Due to the higher exciter current the ohmic voltage drop in the exciter is higher and the exciter flux builds up slower. After about 20 ms T^* is reached and from then on i_e is reduced to the smallest value that allows to hold T^* which reduces ohmic voltage drop in the exciter. As a result one can see that the slope of the exciter flux increases. After the steady state value of ψ_e is reached the currents are steered to their steady state operating values.

The voltage curves show that both methods operate in the same voltage limit. The deviation in the measured exciter voltages and the limit in both methods is proportional to the exciter current and can be explained by voltage drop of the inverter.

VI. Conclusion and Outlook

A novel torque control scheme for EEMSs has been presented along with a real time capable implementation. The test bench results show a significant improvement in torque dynamics. This is enabled by utilization of the magnetic coupling between exciter and stator which can be used to build up exciter current highly dynamic. After set torque is reached the magnetic coupling is used to accelerate the change of the exciter flux. All non-linear magnetic effects of a highly utilized machine are taken into account accurately.

References

[1] M. Märgner and W. Hackmann, “Control challenges of an externally excited synchronous machine in an automotive traction drive application,” in *2010 Emobility - Electrical Power Train*, 2010, pp. 1–6.

[2] O. Haala, B. Wagner, M. Hofmann, and M. Marz, “Optimal current control of externally excited synchronous machines in automotive traction drive applications,” *International Journal of Electrical and Computer Engineering*, vol. 7, no. 9, pp. 1133 – 1139, 2013.

[3] J. Reinhard, K. Löhe, and K. Graichen, “Optimal current setpoint computation for externally excited synchronous machines,” in *2022 IEEE Conference on Control Technology and Applications (CCTA)*, 2022, pp. 1319–1326.

[4] R. Breda, G. Andrioli, S. Calligaro, and R. Petrella, “Extended mtpa and flux-weakening control with total copper loss minimisation and transient torque compensation for wound-rotor synchronous machines,” in *2023 IEEE ECCE*, 2023, pp. 4829–4836.

[5] Y. Kim and K. Nam, “Copper-loss-minimizing field current control scheme for wound synchronous machines,” *IEEE Transactions on Power Electronics*, vol. 32, no. 2, pp. 1335–1345.

[6] J. Stoß, L. Geier, A. Karayel, S. Decker, A. Liske, and M. Hiller, “Unified predictive flux control for eesm, im, pmsm and syrm,” in *2023 IEEE Energy Conversion Congress and Exposition (ECCE)*, 2023, pp. 5009–5019.

[7] S. Goehner, J. Stoss, M. Brodatzki, B. Bachowsky, A. Liske, J. Kolb, and M. Hiller, “New current control strategy for eesms based on the magnetic equivalent circuit with dynamic decoupling of the d- and e-axis,” in *2023 IEEE 8th SPEC/COBEP*, 2023, pp. 1–8.

[8] J. Tang and Y. Liu, “Design of electrically excited synchronous machines to achieve unity power factor in field weakening for long-haul electric trucks,” in *2020 International Conference on Electrical Machines (ICEM)*, vol. 1, 2020, pp. 422–428.

[9] L. Geier, J. Stoß, A. Liske, and M. Hiller, “Analysis of time optimal control strategies for electrically excited synchronous machines using dynamic optimization,” in *2024 IEEE Energy Conversion Congress and Exposition (ECCE)*, 2024.

[10] S. Goehner, J. Stoss, M. Brodatzki, B. Bachowsky, A. Liske, J. Kolb, and M. Hiller, “Identification of rotor position and current dependent flux linkage maps for eesms,” in *2024 IEEE 10th International Power Electronics and Motion Control Conference (IPEMC2024-ECCE Asia)*, 2024, pp. 1996–2003.

[11] A. Brosch, O. Wallscheid, and J. Böcker, “Time-optimal model predictive control of permanent magnet synchronous motors considering current and torque constraints,” *IEEE Transactions on Power Electronics*, vol. 38, no. 7, pp. 7945–7957, 2023.

[12] P. Winzer, “Steigerung von drehmoment und wirkungsgrad bei synchronmaschinen durch nutzung der magnetischen asymmetrie,” Ph.D. dissertation, Karlsruher Institut für Technologie (KIT), 2017.

[13] B. Schmitz-Rode, L. Stefanski, R. Schwendemann, S. Decker, S. Mersche, P. Kiehnle, P. Himmelmann, A. Liske, and M. Hiller, “A modular signal processing platform for grid and motor control, hil and phil applications,” in *2022 International Power Electronics Conference (IPEC-Himeji 2022- ECCE Asia)*, 2022, pp. 1817–1824.